

Cite this article as: Tjørnild MJ, Skov SN, Poulsen KB, Sharghbin M, Benhassen LL, Carlson Hanse L *et al.* Mitral valve posterior leaflet reconstruction using extracellular matrix: an acute porcine study. *Eur J Cardiothorac Surg* 2018; doi:10.1093/ejcts/ezy152.

Mitral valve posterior leaflet reconstruction using extracellular matrix: an acute porcine study†

Marcell J. Tjørnild^{a,b,*}, Søren N. Skov^{a,b}, Karen B. Poulsen^{a,b}, Mona Sharghbin^{a,b}, Leila L. Benhassen^{a,b}, Lisa Carlson Hanse^{a,b}, Farhad Waziri^{b,c}, Diana M. Röpcke^{a,b}, Sten L. Nielsen^{a,b} and J. Michael Hasenkam^{a,b}

^a Department of Cardiothoracic and Vascular Surgery, Aarhus University Hospital, Aarhus, Denmark

^b Department of Clinical Medicine, Aarhus University Hospital, Aarhus, Denmark

^c Department of Cardiology, Aarhus University Hospital, Aarhus, Denmark

* Corresponding author. Department of Cardiothoracic and Vascular Surgery, Aarhus University Hospital, Palle Juul-Jensens Boulevard 99, 8200 Aarhus N, Denmark. Tel: +45-31214223; fax: +45-78453079; e-mail: marcell@clin.au.dk (Marcell Juan Tjørnild).

Received 22 January 2018; received in revised form 7 March 2018; accepted 14 March 2018

Abstract

OBJECTIVES: To investigate mitral valve posterior leaflet and subvalvular reconstruction using a 2-ply small intestinal submucosal extracellular matrix sheet.

METHODS: Mitral valve posterior leaflet and subvalvular reconstruction was characterized in an acute 80-kg porcine model with 7 pigs acting as their own controls. The characterization was based on pressure catheter measurements of pressure differences to identify mitral regurgitation, stenosis and systolic anterior motion. Furthermore, echocardiography was used for the evaluation of leaflet mobility and geometry, whereas sonomicrometry was used to describe annular and subvalvular geometry.

RESULTS: The reconstructed mitral valve was fully functional without any signs of regurgitation (peak left atrial pressure for baseline and reconstruction 12 ± 2 mmHg vs 11 ± 2 mmHg, $P=0.550$), mitral valve stenosis (mean pressure difference across the mitral valve 4.8 ± 2.3 mmHg vs 4.1 ± 2.3 mmHg, $P=0.589$) or systolic anterior motion. The echocardiographic characterization revealed septal–lateral downsizing, reduced tenting area, increased coaptation length (6.0 ± 0.6 mm vs 8.7 ± 2.3 mm, $P=0.002$) and an atrial bend of the reconstructed posterior leaflet. A ballooning effect of the patch material was present at the posterior annular segment.

CONCLUSIONS: Mitral valve posterior leaflet and subvalvular reconstruction using a 2-ply small intestinal submucosal extracellular matrix sheet as patch material was possible in an acute porcine model. The reconstructed mitral valve was fully functional without signs of mitral valve stenosis, valve regurgitation, stenosis or systolic anterior motion. The ballooning appearance of the patch material might, however, constitute an altered leaflet stress distribution in this area.

Keywords: Mitral valve • Mitral valve posterior leaflet • Mitral valve patch repair • Mitral valve posterior leaflet reconstruction • 2-ply small intestinal submucosal extracellular matrix • CorMatrix

INTRODUCTION

Mitral valve repair is generally favoured over mitral valve replacement for primary severe mitral valve regurgitation [1, 2]. This can only be performed when the expected outcome is a durable and fully functional valve and when sufficient pliable mitral valve tissue and chordae tendineae are available [2, 3]. The potential lack of sufficient mitral valve leaflet tissue for mitral valve repair can be observed in rheumatic valve disease, infective endocarditis, congenital heart defects, degenerative mitral valve disease and extensive calcification [4–6]. These diseases are often treated with a patch repair [4, 5]. For a single mitral leaflet repair, an untreated or glutaraldehyde-treated autologous or bovine pericardial patch

has traditionally been used [7]. The techniques rely on good material strength of the remaining native mitral valve material and chordae tendineae [6]. However, patients with extensive mitral leaflet damage might be inappropriate for repair and should instead receive mitral valve replacement [7]. The surgical use of an autologous pericardial patch is also limited by the size of the available patch. In daily practice, these factors limit reconstruction of the entire mitral posterior leaflet and associated chordae tendineae because it requires complex patch repair surgery or mitral valve replacement.

When performing extensive mitral valve patch repair, as with reconstruction of the entire mitral valve, posterior leaflet and associated chordae tendineae, the patch material must not be limited in size. The patch material must be non-infectious, non-thrombogenic, pliable, durable, non-immunogenic and non-calcifying.

†Presented at the 3rd Annual Meeting of the Heart Valve Society, Monte Carlo, Monaco, 2–4 March 2017.

The mechanical properties of such a patch material need to be as physiological as possible, should not shrink over time and preferably not require life-long anticoagulation therapy [8]. It would also be beneficial if the material could be recellularized and contain tissue remodelling properties.

We hypothesize that the 2-ply small intestinal submucosal extracellular matrix has the aforementioned properties and that reconstruction of the entire mitral valve posterior leaflet and associated chordae tendineae is feasible with this material. The aim of this study was to investigate the surgical feasibility and properties of a complete reconstruction of the mitral valve posterior leaflet and associated chordae tendineae using a 2-ply sheet of small intestinal submucosal extracellular matrix in an acute porcine model.

MATERIALS AND METHODS

Animals

Seven pigs comprised the study population in this acute 80-kg porcine model (Mixed Yorkshire and Danish Landrace pigs provided by the University of Aarhus Experimental Animal Farm, Aarhus, Denmark). The porcine anatomical properties are similar to their human counterpart [9]. Three animals had been used for pilot studies and model development prior to this study. All animals were bred under standard laboratory conditions. The study complied with the National Guidelines for Experimental Animal Research, and the study was approved by the Danish Inspectorate of Animal Experimentation.

The patch for mitral valve posterior leaflet and subvalvular reconstruction

The mitral valve posterior leaflet and subvalvular reconstruction patch was made from an 8 × 4 cm 2-ply sheet of small intestinal submucosal extracellular matrix from pigs (CorMatrix[®], Cardiovascular Inc., Alpharetta, GA, USA) (Fig. 1A). The patch was double folded at the annular rim (5 mm) and at the papillary muscle attachment segments (5 × 5 mm), thereby reinforcing the patch material at the site of attachments (Fig. 1B). A 5-0 Prolene[®] suture was used to fixate the double-folded layers. The patch was folded at the papillary muscle fixation points, creating well-defined indentations and P1, P2 and P3 scallops (25 mm, 30 mm and 25 mm, respectively). The P1, P2 and P3 scallop dimensions were created when the patch was attached to the papillary muscles. The patch was oversized at the papillary muscle attachment points, creating an upside down isosceles trapezoid shape of P1 and P3 seen from the side. Our method of implantation cause the P1 and P3 segments on the patch to surrogate for both the chordae tendineae and the P1 and P3 scallops. At the free edge of the P2 scallop, an arc cut-out of 8 mm was made (Fig. 1A), resulting in a height of 22 mm through the P2 midpoint. The arc cut-out was introduced to lower the risk of systolic anterior motion (SAM) of the posterior leaflet. The patch was oversized 0.5–1.0 cm in height, as it allowed the reconstructed posterior leaflet to move towards the anterior leaflet in systole. The circumference was oversized 1.0–2.0 cm, depending on the posterior annulus variation in the animals, as well as to the native mitral valve [10] (Fig. 1C). By oversizing the

circumference, it allowed for the reconstructed posterior leaflet patch to move towards the anterior leaflet in systole.

Instrumentation

Pressure differences across the mitral and aortic valves were measured using the Mikro-Tip pressure catheters (SPR-350S, Millar Instruments, Houston, TX, USA).

Leaflet geometry and mobility were measured with 2-dimensional epicardial echocardiography using a 3-dimensional transoesophageal echocardiographic probe (Vivid E9, GE Vingmed Ultrasound AS, Horten, Norway).

Mitral annular and subvalvular geometry was measured with 11 piezoelectric sonomicrometry crystals (2 mm). The technique is based on ultrasound (Sonometrics Corp., London, Canada) [11]. Eight sonomicrometry crystals were placed around the mitral annulus, 1 on each papillary muscle and 1 at the apex (Fig. 2) [12].

Study design

The study design used was an acute porcine experimental model, where the pigs were investigated before and after mitral valvuloplasty, thus they served as their own controls.

Surgical procedure

Transportation, medication and handling of the animals have previously been described in detail elsewhere [13, 14]. The animals were kept fully anaesthetized during the operation by continuous intravenously infusion of 3.7 mg/h/kg Propofol, 6.2 µg/h/kg Fentanyl and 2.5 mg/h/kg Rocuronium. After baseline epicardial echocardiography and intracardiac and intra-arterial pressure measurements, cardiopulmonary bypass and cardioplegic arrest were established. The native posterior mitral leaflet and the chordae tendineae were then excised through a left atriotomy. On the patch, the P1 segment had 2 connection points for the anterior papillary muscle, and the P3 segment had 2 connection points for the posterior papillary muscle, adding a total of 4 patch and papillary muscle connections (Fig. 1B). Each connection point on the patch was anchored to the papillary muscle attachment site with 3 continuous suture loops using 4-0 Prolene (Fig. 1B). The 3 continuous suture loops spanned over 2–3 mm on the papillary muscle head and the connection point on the patch (Fig. 1B and D). The span between each connection point was approximately 1 cm (Fig. 1B and D). The patch was parachuted down onto the papillary muscles.

Three 4-0 Prolene landmark sutures were placed, 1 at the midpoint of P2 and 1 at each commissure, for the annulus attachment of the patch (Fig. 1C). The oversized patch material was evenly distributed among the 3 landmark sutures and further attached to the annulus, using running inter-locking suture technique. The patch was sutured to the anterior leaflet using a plicated suture at each commissure. The Mikro-Tip pressure catheters were placed in the left ventricle, left atrium and the aorta. The atrium was closed, the animal was weaned from cardiopulmonary bypass, reperfused and a second echocardiography was performed simultaneously with the pressure measurements.

Cardiopulmonary bypass and cardioplegic arrest were instituted for the second time, the left atrium was opened again and the 8 annular and the 3 ventricular sonomicrometry crystals were

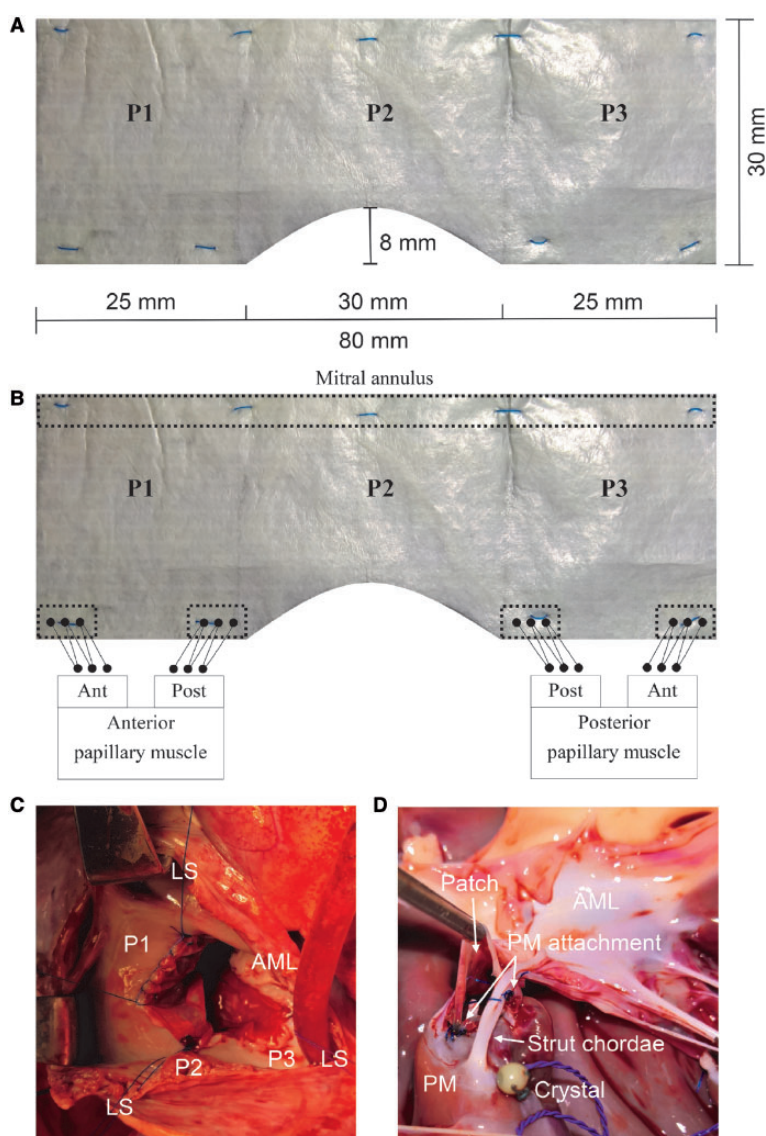


Figure 1: (A and B) Patch for posterior mitral leaflet reconstruction. P1 and P3 also serve as a surrogate for the associated chordae tendineae. Dotted lines mark double folding of the patch material at the mitral annulus (top) and the papillary muscle head (bottom) attachment points. Black circles indicate 3 continuous suture loops at the attachment points between the patch and papillary muscle. Solid rectangular markings represent the anterior and posterior head of the papillary muscles. (C) Intraoperative image showing the annular attachment of the posterior leaflet reconstruction patch using a running locking suture. (D) Postoperative image of the posterior leaflet reconstruction patch attached to the papillary muscle. AML: anterior mitral valve leaflet; Ant: anterior; Crystal: sonomicrometry crystal; LS: landmark suture; P1, P2 and P3: posterior mitral valve scallops; PM: papillary muscle; Post: posterior.

positioned (Fig. 2). The annular sonomicrometry crystal wires were exteriorized through the left atrium, and wires from the ventricular positioned crystals were exteriorized through the apex. The atrium was then closed again, the animal was weaned from cardiopulmonary bypass, re-perfused and the sonomicrometry measurements were performed.

The animals were euthanized under continued anaesthesia with an intravenous injection of an overdose of pentobarbital. The heart was excised, and the sonomicrometry crystal positions were confirmed. All animals were operated by the same surgeon and under the same conditions over a time span of 1 month.

Data acquisition and data analysis

Time derivative of the left ventricular pressure (dLVP/dt) was used for synchronization between the analogue and sonomicrometry

signals. Start systole was defined as the dLVP/dt maximum, mid-systole as the midpoint between dLVP/dt maximum and minimum, end systole as the dLVP/dt minimum, mid-diastole as the midpoint between end systole and the following dLVP/dt maximum and, finally, end diastole as the R-peak in the electrocardiography (ECG).

The signals from the pressure Mikro-Tip catheters were amplified with a pressure control unit (PCU-2000, Millar Instruments) and analysed off-line. The mean mitral valve pressure difference was found between end systole to end diastole. To disclose indication for SAM, the mean aortic valve pressure difference was found between start systole and end systole. A CardioMed system was used for the ECG (Model 4008, CardioMed A/S, Oslo, Norway). All the analogue data signals were recorded using dedicated virtual instrumentation software (LabVIEW 15.0, National Instruments, Austin, TX, USA).

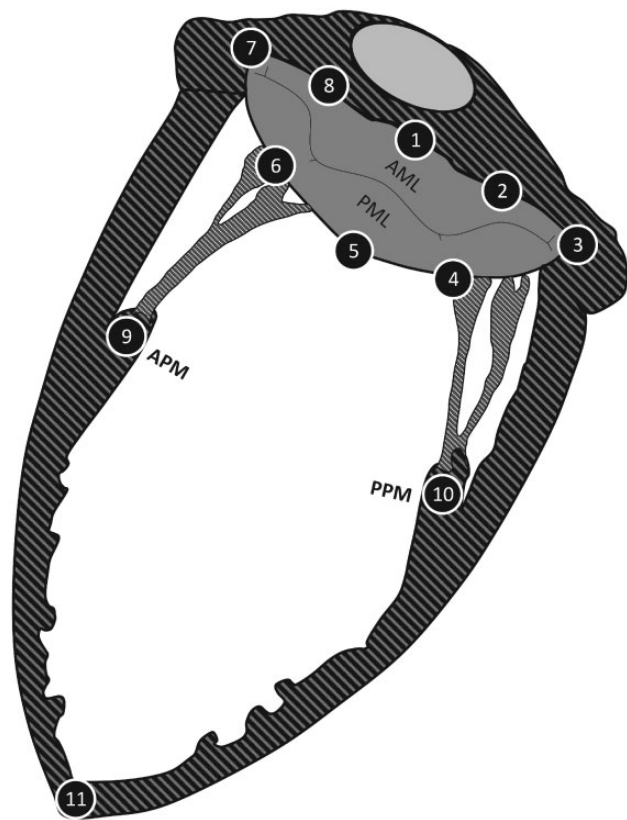


Figure 2: Location of implanted sonomicrometry crystals in the native mitral annulus and the native subvalvular apparatus. The crystal positions were defined by the anatomical landmarks: 1: centre of trigones; 2: right trigone; 3: posterior commissure; 4: P3 scallop; 5: centre of posterior annulus (P2 scallop); 6: P1 scallop; 7: anterior commissure; 8: left trigone; 9: APM; 10: PPM and 11: left ventricular apex. AML: anterior mitral valve leaflet; APM: anterior papillary muscle; PML: posterior mitral valve leaflet; PPM: posterior papillary muscle.

The echocardiographic data were stored for off-line analysis using EchoPAC 113.0.4 (GE Vingmed Ultrasound AS, Horten, Norway). Systole was defined as 1 frame before the S-peak on the ECG and diastole as 1 frame after the T-peak on the ECG. All echocardiographic parameters were measured from inner edge to inner edge. The annulus diameter was divided into an anterior part and a posterior part, with the tenting height as marker. The tenting height was measured from the annulus to the leaflet coaptation. The tenting area for the anterior leaflet and posterior leaflet was measured as the area between the respective leaflet, annular part and tenting height. The total tenting area was calculated by adding the 2 individual areas. The coaptation length was measured as true coaptation in its full length. Billowing height was measured as the distance from the middle of the anterior and posterior annulus part to the respective leaflets and defined as positive in the apical direction. Leaflet length was measured from the annulus to the edge of the leaflet. Ejection fraction was measured at the papillary muscle level in a parasternal short-axis M-mode view, being aware of angle errors. Sufficiency of the valve was verified in a 5-chamber colour Doppler view. All the echocardiographic images were checked for SAM.

The sonomicrometry crystals were connected directly to an external ultrasound transceiver unit. The off-line analyses of inter-crystal distances were post-processed using the multi-dimensional scaling technique for depiction of each crystal in a Cartesian coordinate system (SonoSOFT and SonoXYZ, Sonometrics Corp.,

Table 1: Haemodynamics, cross-clamp time and pressure difference

Parameters	Baseline	PLR	P-value
Heart rate (min^{-1})	78 ± 21	92 ± 11*	0.006*
Peak LVP (mmHg)	85 ± 16	87 ± 15	0.816
Peak of LVP change (dLVP/dt max) (mmHg/s)	1612 ± 639	1587 ± 375	0.911
Peak LAP (mmHg)	12 ± 2	11 ± 2	0.550
Ejection fraction (%)	64 ± 7	68 ± 11	0.322
Cross-clamp time (min)		76 ± 6	
Mitral valve pressure difference mean (mmHg)	4.8 ± 2.3	4.1 ± 2.3	0.589
Aorta valve pressure difference mean (mmHg)	6.8 ± 2.5	6.1 ± 1.8	0.340

Values are presented as mean ± standard deviation.

*P-value <0.05 versus baseline.

dLVP/dt: time derivative of the left ventricular pressure; LAP: left atrial pressure; LVP: left ventricular pressure; PLR: posterior mitral leaflet reconstruction.

London, Canada). The mitral annular circumference was calculated as the summarized distance between the 8 annular crystals. The mitral annular area was calculated as the summarized area of the 8 adjacent triangular areas. The inter-crystal distance of 2 adjacent crystals was used to identify local variations. The direct septal-lateral distance was calculated between Crystal 1 to Crystal 5, commissure–commissure distance between Crystal 3 and Crystal 7 and papillary muscle distance between Crystal 9 and Crystal 10 (Fig. 2). The anterior segment was calculated as the distance between Crystal 7 and Crystal 3 following the anterior part of the mitral annulus and the posterior segment between Crystal 3 and Crystal 7 following the posterior part of the mitral annulus. A least square plane was made from the annular crystals to calculate individual annular crystal height to the least square plane, as an indicator of the mitral saddle shape. The annular height was calculated as the sum of the highest crystal-plane distances on each side of a least-square plane. Furthermore, the ratio between the annular height and commissure–commissure distance was expressed in terms of the annular height-to-commissural width ratio.

Statistical analysis

All data are reported as mean ± standard deviation and analysed using STATA version 13 (StataCorp LP, College Station, TX, USA) with a significance level of $P < 0.05$. Development of the statistical models was performed with support from the Aarhus University (BIAS, University of Aarhus, Aarhus, Denmark). Haemodynamic and sonomicrometry parameters were compared using a mixed model, by means of measurement point and repetitive heart cycle as factors. Echocardiographic parameters were compared with another mixed model, using groups as a factor. Both models allowed for different residual variations between measurement points. Visual diagnostics were used to verify normal distribution and inspection of the model residuals, and fitted values did not give cause to doubt these models. Groups from both models were finally compared using the *post hoc* Wald z-tests.

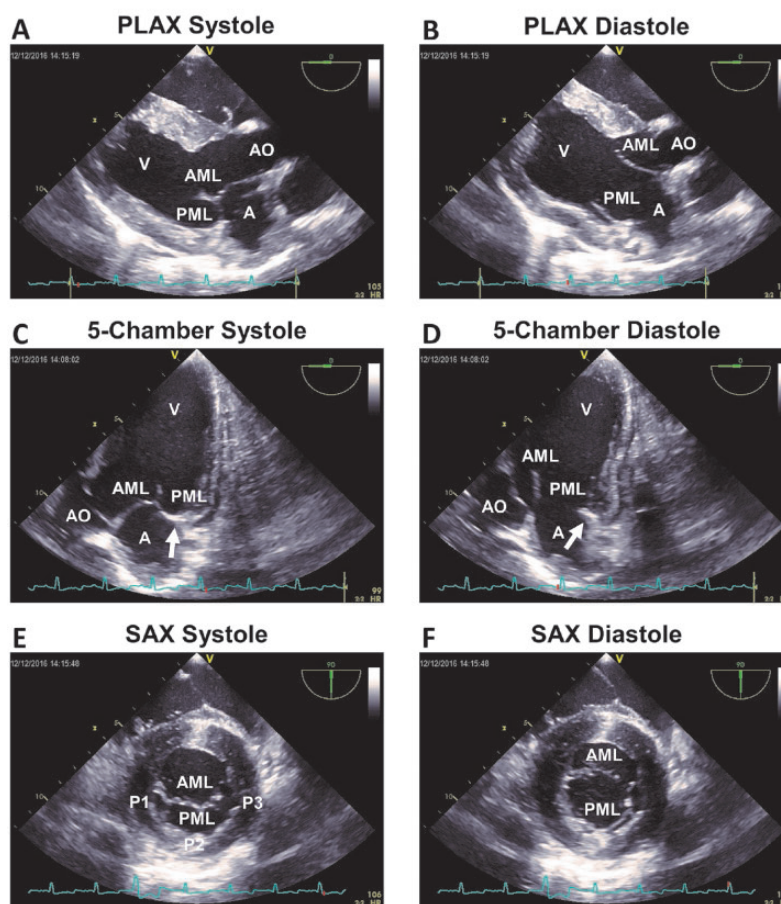


Figure 3: Echocardiographic images of the mitral posterior leaflet reconstruction in both systole and diastole. All echocardiographies were performed on the epicardium. Arrows indicate the patch part with ballooning effect. A: left atrium; AML: anterior mitral valve leaflet; AO: aorta; P1, P2 and P3: posterior mitral valve scallops; PML: posterior mitral valve leaflet; PLAX: parasternal long axis; SAX: parasternal short axis; V: left ventricle.

RESULTS

Haemodynamic results

The haemodynamic data, cross-clamp time, aortic valve and mitral valve pressure differences are presented in Table 1. There was no change in peak left atrial pressure (12 ± 2 mmHg vs 11 ± 2 mmHg) or mean pressure difference across the mitral valve (4.8 ± 2.3 mmHg vs 4.1 ± 2.3 mmHg) before and after reconstruction. The mitral valve was fully functional without any signs of regurgitation, mitral valve stenosis or SAM.

Echocardiographic results

Repre images are shown in Fig. 3, and parameters are listed in Table 2. The echocardiographic video of the posterior leaflet reconstruction in a long-axis view can be seen in Video 1 and a short-axis view in Video 2. Echocardiographic assessment revealed a fully functional valve in all animals, without regurgitation and with similar ejection fractions ($64 \pm 7\%$ vs $68 \pm 11\%$), after mitral valve posterior leaflet and subvalvular reconstruction. The reconstruction significantly reduced the mitral annulus septal-lateral diameter and tenting area for both the anterior and posterior leaflets. A statistically significant lower billowing height was observed in the posterior leaflet, indicating an atrial bend

instead of a ventricular bend of the reconstructed posterior leaflet. A statistically significantly increased coaptation length was observed for the posterior leaflet length.

Sonomicrometry results

Mitral annular geometric results for mitral annular area, mitral annular circumference, septal-lateral distance and commissure-commissure distance are shown in Fig. 4. The cyclic papillary muscle distance, anterior and posterior annular segment distances, annular height and annular height-to-commissural width ratio are shown in Fig. 5. The annular crystal distances at end systole to the least square plane as an expression of saddle shape of the mitral annulus are also shown in Fig. 5. Annular segmental circumferential changes from end diastole to end systole, as an expression of the regional systolic circumferential changes, are illustrated with a scaled colour legend in Fig. 6.

DISCUSSION

We successfully performed mitral valve posterior leaflet and subvalvular reconstruction in an acute porcine model using a single 2-ply small intestinal submucosal extracellular matrix patch. The valve was fully functional immediately after surgery and with a

Table 2: Echocardiographic parameters in an apical 5-chamber view

Parameters	Baseline	PLR	P-value
Annulus diameter (SL) (mm)			
Systole	27.0 ± 2.1	21.0 ± 0.6*	0.000*
Diastole	29.9 ± 2.1	23.3 ± 1.6*	0.000*
Cyclic change	2.9 ± 0.7	2.3 ± 1.7	0.411
Systole anterior leaflet part			
Systole posterior leaflet part	10.7 ± 0.8	8.6 ± 2.2*	0.004*
Tenting height (mm)			
Tenting area (mm ²)	142.9 ± 16.0	105.7 ± 23.0*	0.000*
Anterior leaflet part			
Posterior leaflet part	44.3 ± 5.3	31.4 ± 10.7*	0.004*
Coaptation length (mm)			
Billowing height (mm)	6.0 ± 0.6	8.7 ± 2.3*	0.002*
Anterior leaflet			
Posterior leaflet	8.1 ± 0.7	7.0 ± 2.2	0.138
Posterior leaflet			
Anterior leaflet	4.6 ± 0.5	3.4 ± 0.5*	0.000*
Leaflet length (mm)			
Anterior leaflet	24.1 ± 1.6	24.3 ± 1.6	0.317
Posterior leaflet	17.6 ± 1.6	20.0 ± 1.3*	0.005*

Values are presented as mean ± standard deviation. Billowing height is defined as positive in the apical direction.

*P-value <0.05 versus baseline.

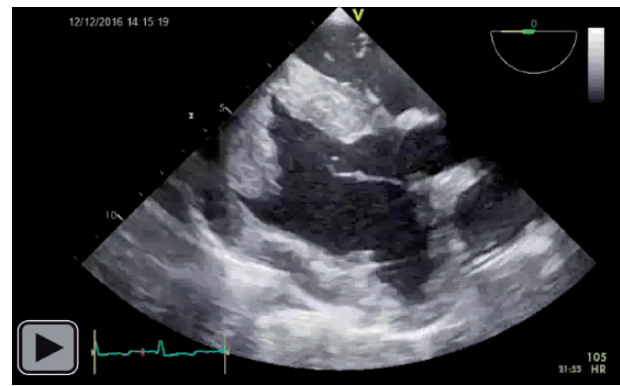
PLR: posterior mitral leaflet reconstruction; SL: septal-lateral.

cross-clamp time of 76 ± 6 min, making this procedure feasible for the clinical setting. The 8 × 4-cm patch was made with an arc cut-out at P2 and double-folded layers at both the annular and the papillary muscle attachment points (Fig. 1A and B).

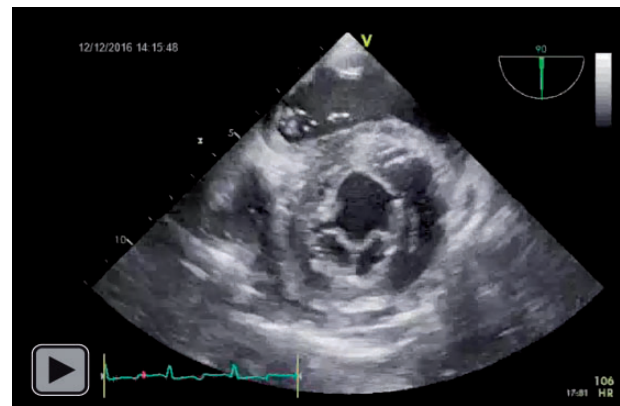
The reconstruction was fully functional and without regurgitant jets on the colour Doppler echocardiography. This was confirmed with similar peak left atrial pressure for baseline and reconstruction (12 ± 2 mmHg vs 11 ± 2 mmHg). The reconstruction did not cause any indication for stenosis with similar mean pressure difference across the mitral valve (4.8 ± 2.3 mmHg vs 4.1 ± 2.3 mmHg). Signs of SAM on echocardiography (Fig. 3) were not observed, which was confirmed with similar catheter-based mean pressure difference across the aortic valve (6.8 ± 2.5 mmHg vs 6.1 ± 1.8 mmHg).

From the echocardiographic analysis of the posterior leaflet reconstruction, we found that the reconstruction had similar anatomical and functional appearances as the native mitral valve (Fig. 3). The overall echocardiographic parameters were furthermore comparable with the human heart [15]. However, the mitral annulus was statistically significantly downsized in systole and diastole when compared with baseline (Table 2). A similar systolic contraction of the mitral annulus indicates similar cyclic dynamics before and after the reconstruction procedure, despite the overall downsizing according to the patch dimensions and attachment to the mitral annulus.

The mitral annular downsizing led to a statistically significant smaller tenting area, together with a similar tenting height, indicating a changed leaflet configuration. The billowing height of the native anterior leaflet was unchanged, whereas the reconstructed posterior leaflet revealed a statistically significant lower billowing height. The atrial bend of the posterior leaflet (and hence lower billowing height) could be caused by a surplus of tissue and the lack of intermediate or basal chordae tendineae to



Video 1: Long-axis echocardiographic view of posterior leaflet reconstruction.



Video 2: Short-axis echocardiographic view of posterior leaflet reconstruction.

counteract the systolic pressure pushing the leaflet towards the atrium.

The maximum changes, minimum changes and changes in mitral annular area, mitral annular circumference and commissure-commissure distance (Fig. 4A and C) confirmed an overall compatibility of size and dynamics when compared with similar native studies [12, 16, 17]. The systolic saddle shape was preserved with the reconstruction (Fig. 5C) together with a physiological cyclic change in annular height-to-commissural width ratio and annular height (Fig. 5D), as observed in similar native studies [16, 18]. The anterior annular segment kept its physiological systolic expansion after reconstruction (Figs 5B and 6), as found in other studies [12, 16, 17]. The inter-papillary muscle distance and dynamics (Fig. 5A) were comparable with similar native studies after reconstruction [19].

The septal-lateral distance was measured both with echocardiography and sonomicrometry. Both showed an overall septal-lateral downsizing when compared with baseline and similar native studies [12, 16, 17]. This indicates that the patch material was elastic at the mitral annulus and made a ballooning effect with systolic widening (Fig. 3C, arrow). This ballooning effect with systolic widening is also observed in the mitral annular area, mitral annular circumference and commissure-commissure distance (Fig. 4B and D). This is confirmed with a systolic widening of the posterior segment (Fig. 5B) and the individual segmental circumferential changes (Fig. 6). The ballooning effect may

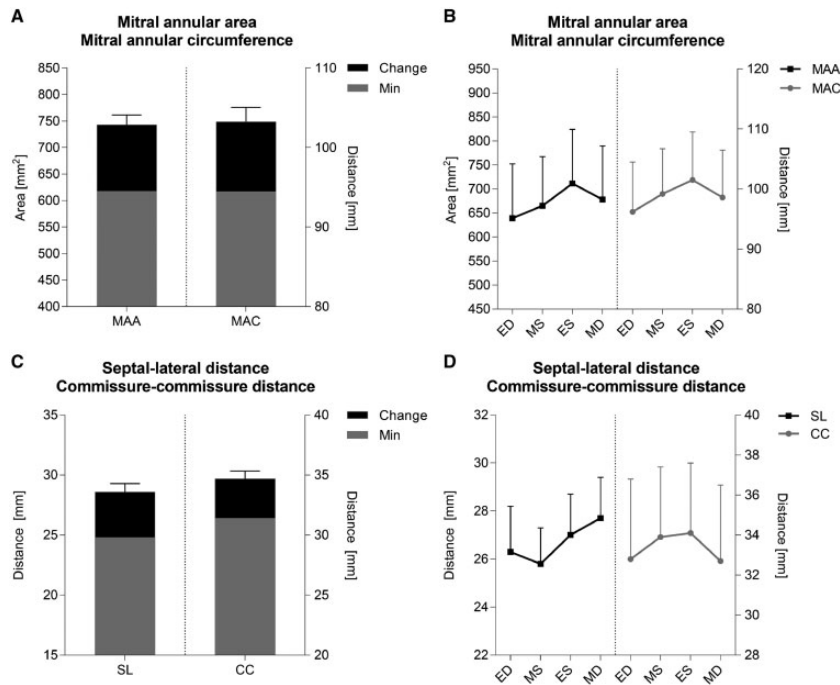


Figure 4: (A and C) Maximal, minimal and change values with standard deviation in MAA, MAC, SL distance and CC distance. (B and D) Absolute values with standard deviations for the same parameters used in (A) and (C), at 4 defined time points throughout the cardiac cycle. CC: commissure-commissure; ED: end diastole; ES: end systole; MAA: mitral annular area; MAC: mitral annular circumference; MD: mid-diastole; MS: mid-systole; SL: septal-lateral.

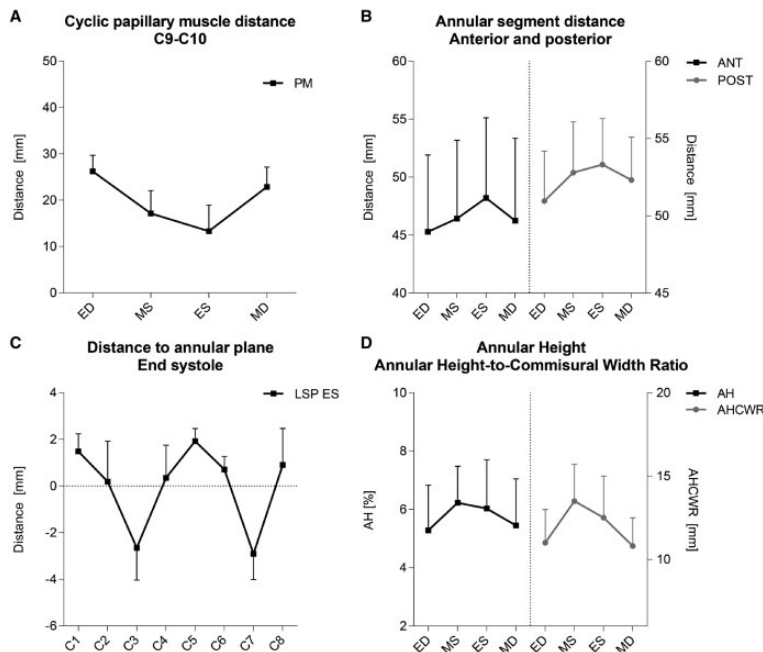


Figure 5: (A) Inter-papillary muscle distance from Crystal 9 to Crystal 10. (B) Mitral annular circumferential distance divided into an anterior segment, between Crystal 7 and Crystal 3 following the anterior part of the mitral annulus and a posterior segment between Crystal 3 and Crystal 7 following the posterior part of the mitral annulus. (C) Annular crystal distance to the LSP, as an expression of the mitral saddle shape, in end systole. (D) AHCWR and AH. Absolute values with standard deviations at 4 defined time points throughout the cardiac cycle (A, B, D). AH: annular height; AHCWR: annular height-to-commissural width ratio; Ant: anterior; ED: end diastole; ES: end systole; LSP: least square plane; MD: mid-diastole; MS: mid-systole; Post: posterior; PM: papillary muscle.

originate from systolic filling of the P1, P2 and P3 scallops (Fig. 3E). These scallops were created using the 1–2 cm oversized patch at the attachment points on the papillary muscle heads and 0.5–1 cm oversized height of the patch. Leaflet billowing changed ‘radius of curvature’ and hereby leaflet stress distribution

in this area, which might have implications for the tissue remodelling over time. It is plausible that a smaller patch could reduce the billowing of the patch extension; however, it could be on expense of patch dehiscence and/or inappropriate leaflet apposition.

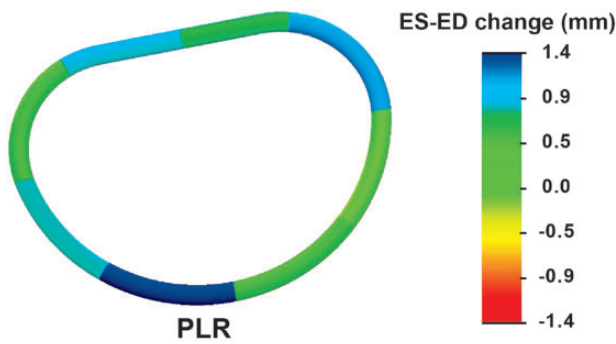


Figure 6: Circumferential changes of the annular segment after posterior leaflet reconstruction from end diastole to end systole illustrated with a scaled colour legend. Blue represents a systolic annular expansion and red represents a systolic annular compression. ED: end diastole; ES: end systole; PLR: posterior mitral leaflet reconstruction.

Further investigations are needed to check whether a mitral annuloplasty ring will counteract this ballooning effect. Another option is to make a more restrictive patch, with a smaller circumference and smaller height, however, thereby risking a fully restrictive posterior leaflet and regurgitation. Furthermore, this might also lead to more tension on the patch from the papillary muscle to the annulus, with the risk of dehiscence or rupture.

We used a patch of 2-ply small intestinal submucosal extracellular matrix from pigs. However, any patch material with the same biomechanical properties could have been used. If the material has other biomechanical properties, then some of the findings may differ. We found that the 2-ply small intestinal submucosal extracellular matrix material was pliable and functional for this mitral valve posterior leaflet and subvalvular reconstruction. Signs of tearing or rupture of the tissue were not observed. However, the long-term effects still need investigation. The recellularization perspective of this new 2-ply version of small intestinal submucosal extracellular matrix also needs further investigation. Nevertheless, the results from this study seem to be promising, and it might be applicable in a clinical setting.

The clinical perspective with this novel reconstruction technique and the material used, or other materials with the same biomechanical properties, is reconstruction of the posterior mitral valve leaflet even after total degeneration of the native leaflet material as observed in extensive calcification or rheumatic valve disease. Size and configuration were standardized in this acute porcine model. In future, for the clinical application of this approach to mitral leaflet reconstruction, individualized sizing and configuration will be required.

Limitations

The results must be interpreted by considering the limitations of this study. All data were collected in an acute healthy open-chest porcine model directly after complicated cardiac surgery. Pathophysiological deformities of the mitral valve or the left ventricular chamber were not observed, as observed in patients with a mitral incompetence component. Translation of the results, directly to the clinical situation, should be performed with caution. Because of the limited number of animals and acute setting, the study does not provide any results regarding long-term effects.

CONCLUSIONS

Mitral valve posterior leaflet and subvalvular reconstruction using a 2-ply small intestinal submucosal extracellular matrix sheet as patch material was feasible in an acute porcine model. The reconstructed mitral valve was fully functional without signs of mitral valve regurgitation, stenosis or systolic anterior motion. The ballooning appearance of the patch material might constitute an altered leaflet stress distribution in this area.

Funding

This work was supported by the Lundbeck Foundation [Grant number R184-2014-2478], the Danish Heart Foundation [Grant numbers 16-R107-A6588-22041 and 16-R107-A6588-22042], the Graduate School, Health, Aarhus University [Grant number 18931909] and the Helga and Peter Korning Foundation.

Conflict of interest: The 2-ply version of small intestinal submucosal extracellular matrix material was donated by CorMatrix.

REFERENCES

- [1] Nishimura RA, Otto CM, Bonow RO, Carabello BA, Erwin JP, Fleisher LA *et al.* 2017 AHA/ACC focused update of the 2014 AHA/ACC guideline for the management of patients with valvular heart disease: a report of the American College of Cardiology/American Heart Association Task Force on Clinical Practice Guidelines. *J Am Coll Cardiol* 2017;70:252–89.
- [2] Baumgartner H, Falk V, Bax JJ, Bax JJ, De Bonis M, Hamm C *et al.* 2017 ESC/EACTS guidelines for the management of valvular heart disease. *Eur Heart J* 2017;38:2739–91.
- [3] Ito T, Maekawa A, Aoki M, Hoshino S, Hayashi Y, Sawaki S *et al.* Seamless reconstruction of mitral leaflet and chordae with one piece of pericardium. *Eur J Cardiothorac Surg* 2014;45:e227–32.
- [4] Feindel CM, Tufail Z, David TE, Ivanov J, Armstrong S. Mitral valve surgery in patients with extensive calcification of the mitral annulus. *J Thorac Cardiovasc Surg* 2003;126:777–82.
- [5] Uchimuro T, Fukui T, Shimizu A, Takashi S. Mitral valve surgery in patients with severe mitral annular calcification. *Ann Thorac Surg* 2016; 101:889–95.
- [6] Shomura Y, Okada Y, Nasu M, Koyama T, Yuzaki M, Murashita T *et al.* Late results of mitral valve repair with glutaraldehyde-treated autologous pericardium. *Ann Thorac Surg* 2013;95:2000–5.
- [7] Habib G, Lancellotti P, Antunes MJ, Bongiorni MG, Casalta JP, Del Zotti F *et al.* 2015 ESC Guidelines for the management of infective endocarditis: the task force for the management of infective endocarditis of the European Society of Cardiology (ESC). Endorsed by: European Association for Cardio-Thoracic Surgery (EACTS), the European Association of Nuclear Medicine (EANM). *Eur Heart J* 2015;36:3075–128.
- [8] Schöll FG, Boucek MM, Chan KC, Valdes-Cruz L, Peryman R. Preliminary experience with cardiac reconstruction using decellularized porcine extracellular matrix scaffold: human applications in congenital heart disease. *World J Pediatr Congenit Heart Surg* 2010;1:132–6.
- [9] Lelovas PP, Kostomitsopoulos NG, Xanthos TT. A comparative anatomic and physiologic overview of the porcine heart. *J Am Assoc Lab Anim Sci* 2014;53:432–8.
- [10] Dal-Bianco JP, Levine RA. Anatomy of the mitral valve apparatus: role of 2D and 3D echocardiography. *Cardiol Clin* 2013;31:151–64.
- [11] Gorman JH, Gupta KB, Streicher JT, Gorman RC, Jackson BM, Ratcliffe MB *et al.* Dynamic three-dimensional imaging of the mitral valve and left ventricle by rapid sonomicrometry array localization. *J Thorac Cardiovasc Surg* 1996;112:712–26.
- [12] Skov SN, Røpcke DM, Tjørnild MJ, Ilkjær C, Rasmussen J, Nygaard H *et al.* The effect of different mitral annuloplasty rings on valve geometry and annular stress distribution. *Interact CardioVasc Thorac Surg* 2017;24: 683–90.

- [13] Nielsen SL, Lomholt M, Johansen P, Hansen SB, Andersen NT, Hasenkam JM. Mitral ring annuloplasty relieves tension of the secondary but not primary chordae tendineae in the anterior mitral leaflet. *J Thorac Cardiovasc Surg* 2011;141:732–7.
- [14] Ropcke DM, Ilkjær C, Skov SN, Tjørnild MJ, Sørensen AV, Jensen H *et al.* Functional and biomechanical performance of stentless extracellular matrix tricuspid tube graft: an acute experimental porcine evaluation. *Ann Thorac Surg* 2016;101:125–32.
- [15] Dwivedi G, Mahadevan G, Jimenez D, Frenneaux M, Steeds RP. Reference values for mitral and tricuspid annular dimensions using two-dimensional echocardiography. *Echo Res Pract* 2014;1:43–50.
- [16] Skov SN, Ropcke DM, Tjørnild MJ, Ilkjaer C, Rasmussen J, Nygaard H *et al.* Remodeling mitral annuloplasty ring concept with preserved dynamics of annular height. *J Heart Valve Dis* 2017;26:295–303.
- [17] Rausch MK, Bothe W, Kvitting JP, Swanson JC, Ingels NB, Miller DC *et al.* Characterization of mitral valve annular dynamics in the beating heart. *Ann Biomed Eng* 2011;39:1690–702.
- [18] Timek TA, Glasson JR, Lai DT, Liang D, Daughters GT, Ingels NB *et al.* Annular height-to-commissural width ratio of annuloplasty rings in vivo. *Circulation* 2005;112:1423–8.
- [19] Jensen H, Jensen MO, Smerup MH, Ringgaard S, Sorensen TS, Andersen NT *et al.* Three-dimensional assessment of papillary muscle displacement in a porcine model of ischemic mitral regurgitation. *J Thorac Cardiovasc Surg* 2010;140:1312–18.